Self-assembling toxin-based nanoparticles as self-delivered antitumoral drugs

Laura Sánchez-García [a,b,c,†], Naroa Serna [a,b,c,†], Patricia Álamo [c,d,e], Rita Sala [c,d], María Virtudes Céspedes [c,d], Mònica Roldan [f], Alejandro Sánchez-Chardi [g], Ugutz Unzueta [c,d], Isolda Casanova [c,d,e], Ramón Mangues [c,d,e,*], Esther Vázquez [a,b,c], Antonio Villaverde [a,b,c,*]

[a] Institut de Biotecnologia i de Biomedicina, Universitat Autònoma de Barcelona, Bellaterra, 08193 Barcelona, Spain

[b] Departament de Genètica i de Microbiologia, Universitat Autònoma de Barcelona, Bellaterra, 08193 Barcelona, Spain

[c] CIBER de Bioingeniería, Biomateriales y Nanomedicina (CIBER-BBN), Spain

[d] Institut d'Investigacions Biomèdiques Sant Pau, Hospital de la Santa Creu i Sant Pau, 08025 Barcelona, Spain

[e] Josep Carreras Research Institute, Hospital de la Santa Creu i Sant Pau, Barcelona, Spain

[f] Unitat de Microscòpia Confocal. Servei d'Anatomia Patològica, Institut Pediàtric de Malalties Rares (IPER). Hospital Sant Joan de Déu, Edifici Consultes Externes. Passeig Sant Joan de Déu, 2, Planta 0, 08950 Esplugues de Llobregat, Barcelona

[g] Servei de Microscòpia, Universitat Autònoma de Barcelona, Bellaterra, 08193 Barcelona, Spain

[†] Equally contributed.

[*] Corresponding authors. RM: rmangues@santpau.cat; AV: antoni.Villaverde@uab.es

Keywords: Protein materials; nanoparticles; drug delivery; cell-targeting; recombinant proteins

Abstract

Loading capacity and drug leakage from vehicles during circulation in blood is a major concern when developing nanoparticle-based cell-targeted cytotoxics. To circumvent this potential issue it would be convenient the engineering of drugs as self-delivered nanoscale entities, devoid of any heterologous carriers. In this context, we have here engineered potent protein toxins, namely segments of the diphtheria toxin and the *Pseudomonas aeruginosa* exotoxin as self-assembling, self-delivered therapeutic materials targeted to $CXCR4^+$ cancer stem cells. The systemic administration of both nanostructured drugs in a colorectal cancer xenograft mouse model promotes efficient and specific local destruction of target tumor tissues and a significant reduction of the tumor volume. This observation strongly supports the concept of intrinsically functional protein nanoparticles, which having a dual role as drug and carrier, are designed to be administered without the assistance of heterologous vehicles.

1 Introduction

Natural protein toxins are produced by different species of unicellular and pluricellular organisms and are extremely potent functional molecules [1]. Toxins occur alone or as venom components with roles in predation and defense or during tissue colonization in bacterial infections and show a wide spectrum of mechanisms of action that target vital physiological processes. The biological properties of protein toxins can be exploited in a therapeutic context, because they are usually preserved in versions produced by recombinant DNA technologies. This fact allows the industry-oriented, large-scale bioproduction and further formulation of protein toxins as medicines. A few toxin-based drugs have been already approved for use in humans by the medicament agencies, including Captopril for hypertension, Prialt for chronic pain, Integrilin for coronary angioplasty, Byetta for type 2 diabetes, Botox for neuromuscular disorders and Contulakin-G as an analgesic [2-6]. Many others are currently under development or in clinical trials [7-9]. A major therapeutic value of toxins relies on their ability to kill exposed cells through molecular events that are devoid, in general, of cell type specificity. The high potency exhibited by some toxins enables toxin-mediated cell killing to be explored in oncology to replace or complement conventional chemotherapies [10, 11]. However, not only efficient but selective cell killing should be envisaged when developing antitumoral drugs, to minimize the undesired adverse effects and potentially severe toxicity associated to conventional chemotherapies. As an example, in the drug Denileukin diftitox, cell targeting is provided by the human interleukin-2. Fused to the fragments A and B of the *Corynebacterium diphtheriae* exotoxin (diphtheria toxin), this cytokine allows binding of the whole fusion to the IL-2 receptor, overexpressed in cutaneous T cell lymphoma cells. Ideally, toxins for use in oncology should be targeted by highly specific ligands of tumoral surface markers [12-15] and administered in stable formulations ensuring bioavailability and minimizing renal filtration. This would be achieved by presenting them in sizes over the renal clearance threshold (~ 8 nm), through the use of nanoscale carriers. Regarding the extremely high potency of toxins, possible drug leakage from the vehicle during blood circulation represents an important risk that limits the development of toxin-based

nanoconjugates. In addition, the intrinsic potential toxicity of the nanoparticle used as carrier, is a matter of additional concern at both individual and environmental levels [16, 17]. In this regard, the current trends towards developing self-delivery nanoscale drugs devoid of heterologous vehicles [18] might potentially expand the fields or applicability of toxins and other cytotoxic protein drugs in safer ways. However, the first prototypes in this line have resulted in very complex combinations of different types of molecules, that devoid of true nanoscale vehicles, require instead the assistance of accompanying molecular systems to provide the required functions. For instance, self-assembling therapeutic siRNA has been combined with polymeric metformin, condensed with hyaluronic acid and the nanoparticles covered with 1,2-dioleoyl-3-tri-methylammonium-propane chloride and cholesterol and functionalized with a sigma receptor ligand [19]. As another recent example, the anticancer agent epigallocatechin gallate was induced to self-assemble in combination with the antitumoral proteins herceptin or interferon alpha-2a (IFN-a 2a), followed by coating with polyethylene glycol [20].

In contrast to the chemical heterogeneity of these constructs, that are observed as representative of vehicle-free nanomedicines [18], the emerging concept of self-delivered nanoscale drugs could be fully achieved by functional recruitment in single molecular species that such as proteins, can oligomerize as chemically homogeneous nanoscale entities with predefined properties [21]. Importantly, nanoscale size in drug formulations is of high clinical relevance as cell penetrability and drug stability are favoured, the enhanced permeability and retention (EPR) effect stimulated and renal clearance largely minimized [18, 22]. Recently [23], we have proposed a biological principle to promote self-assembling of fusion proteins as stable protein-only nanoparticles using cationic end-terminal tags. In addition, we have proved that short protein segments, such as pro-apoptotic or antimicrobial peptides, might retain their therapeutic potential when fused to carrier proteins such as GFP and once organized in oligomers [24]. Then, a protein toxin might be genetically instructed, by the addition of architectonic and cell targeting tags, to self-assemble into stable nanoparticles acting as intrinsically functional, cell-targeted protein materials with self-delivery properties. In this context, we have here engineered two potent toxins as CXCR4-targeted self-

assembling nanoparticles for the systemic treatment of $CXCR4^+$ colorectal cancer. These proteins are the active fragments of the diphtheria toxin and of the *Pseudomonas aeruginosa* exotoxin, that perform ADP-ribosylation of the elongation factor 2 (EF-2), resulting in the irreversible inhibition of protein synthesis and cell death [25, 26]. In addition, we designed these drug biomaterials to proteolytically discharge the targeting agent and other non-relevant protein segments upon cell internalization, for the cytotoxic activity being solely executed by the precise protein drug domain.

2. Materials and Methods

2.1 Protein design, production, purification and characterization

Synthetic genes encoding the self-assembling modular proteins T22-DITOX-H6 and T22-PE24-H6 respectively were designed in-house (Figure 1A) and provided by Geneart (ThermoFischer). DITOX contains the translocation and catalytic domains of the diphtheria toxin from *Corynebacterium diphtheriae*. PE24 is based in the de-immunized catalytic domain of *Pseudomonas aeruginosa* exotoxin A in which point mutations that disrupt B and T cell epitopes have been incorporated. Moreover, it has been added a KDEL sequence in the C-terminus of T22-PE24-H6, which enables the binding to KDEL receptors more efficiently at the Golgi apparatus during subsequent intracellular trafficking [27]. Furin-cleavage sites were inserted between the CXCR4 ligand T22 and the functional toxin (Figure 1A) to release the amino terminal peptide once internalized into target cells. This has been designed so as the natural version of both toxins act with free amino termini [26, 28], and the recombinant versions proved to be active also show this terminal end in absence of additional peptide segments [29, 30]. Both gene fusions were inserted into the plasmid pET22b, and the recombinant versions of the vector were transformed by heat shock in *Escherichia coli* Origami B (BL21, $OmpT^-$, Lon^-, $TrxB^-$, Gor^-, Novagen, Darmstadt, Germany). Transformed cells were grown at 37 ºC overnight in LB medium supplemented with 100 µg/ml ampicillin, 12.5 µg/ml tetracycline and 15 µg/ml kanamycin. The encoded proteins were produced at 20 ºC overnight upon addition of 0.1 and 1 mM IPTG (isopropyl-β-D-thiogalactopyronaside) for T22-DITOX-H6 and T22-PE24-H6 respectively, when the OD_{550} of the cell culture reached around 0.5-0.7. Bacterial cells were centrifuged during 15 min (5,000 g at 4 ºC) and kept at -80 ºC until use. Pellets were thaw and resuspended in Wash buffer (20 mM Tris-HCl pH 8.0, 500 mM NaCl, 10 mM imidazole) in presence of protease inhibitors (Complete EDTA-Free, Roche Diagnostics, Indianapolis, IN, USA). Cell disruption was performed by French Press (Thermo FA-078A) at 1200 psi. The lysates were then centrifuged for 45 min (15,000 g at 4 ºC), and the soluble fraction was filtered using a pore diameter of 0.2 µm.

Proteins were then purified through the His-tag by Immobilized Metal Affinity Chromatography (IMAC) using a HiTrap Chelating HP 1 ml column (GE Healthcare, Piscataway, NJ, USA) with an AKTA purifier FPLC (GE Healthcare). Elution was achieved

using a lineal gradient of Elution buffer (20 mM Tris-HCl pH 8.0, 500 mM NaCl and 500 mM imidazole). The eluted fractions were collected, dialyzed against carbonate buffer (166 mM $NaCO_3H$ pH 8) and centrifuged for 15 min (15,000 g at 4 ºC) to remove insoluble aggregates. The integrity and purity of the proteins was analyzed by mass spectrometry (MALDI-TOF), SDS-PAGE and Western blotting using anti-His monoclonal antibody (Santa Cruz Biotechnology, Santa Cruz, CA, USA). Protein concentration was determined by Bradford's assay. The nomenclature used for the fusion proteins has been established according to their modular organization.

2.2 Furin cleavage design and detection

To promote the intracellular release of ligand-free toxins, two different furin cleavage sites, naturally acting in the respective toxin precursors to activate translocation, were included in T22-DITOX-H6 and T22-PE24-H6 (Figure 1A). Efficiency of cleavage in the platform was assessed in T22-DITOX-H6, since the expected fragments should exhibit fully distinguishable molecular masses suitable for quantitative analysis. For that, HeLa cell extracts exposed to 1 µM protein for 24 h were submitted to a Western Blot analysis. After protein incubation, cells were collected, centrifuged, suspended in DPBS and disrupted by sonication. The Western Blot bands were quantified using Image Lab Software version 5.2.1. Two additional modular proteins were also constructed in which these engineered furin cleavage sites were not included, namely T22-DITOX-H6 F^- and T22-PE24-H6 F^-. Their amino acid sequence exactly matched that of the equivalent constructs T22-DITOX-H6 and T22-PE24-H6 at exception of the boldface dark blue peptide (Figure 1 A), corresponding to the protease target site. These non-cleavable constructs were used for a comparative analysis of protein cytotoxicity.

2.3 Fluorescence labelling and dynamic light scattering

T22-DITOX-H6 and T22-PE24-H6 were labelled with ATTO 488 (Sigma Aldrich, Buchs, Switzerland) to track their internalization when performing *in vitro* and *in vivo* experiments. The conjugation was performed at a molar ratio of 1:2 at room temperature in darkness. The reaction mixture was gently stirred every 15 min during 1 h, centrifuged for 15 min (15,000 g at 4 ºC) and dialyzed overnight in the original buffer (166 mM $NaCO_3H$ pH 8) to eliminate free ATTO. Fluorescence of the

nanoparticles at 0.1 mg/ml was determined by a Varian Cary Eclipse fluorescence spectrophotometer (Agilent Technologies, Mulgrave, Australia) at 523 nm using an excitation wavelength of 488 nm. For comparative analyses, the intensity of fluorescence was corrected by protein amounts to render specific emission values. Stability of dye conjugation was assessed through the incubation of T22-DITOX-H6* at a final concentration of 0.5 µg/µL in human serum (S2257-5ML, Sigma, St Louis, MO, USA) for 48 h at 37 °C, with gentle agitation. Then, the sample was dialyzed in 300 ml of carbonate buffer (166 mM $NaCO_3H$, pH 8) for 2 h to remove the free ATTO that might have been released from the nanoparticle. In parallel a positive control was dialyzed containing the same amount of free ATTO. The fluorescence of buffers obtained after the dialysis was measured in the fluorimeter. The volume size distribution of all nanoparticles was determined by dynamic light scattering (DLS) at 633 nm (Zetasizer Nano ZS, Malvern Instruments Limited, Malvern, Worcestershire, UK).

2.4 Ultrastructural characterization

Size and shape of T22-DITOX-H6 and T22-PE24-H6 nanoparticles at nearly native state were evaluated with a field emission scanning electron microscope (FESEM) Zeiss Merlin (Zeiss, Oberkochen, Germany) operating at 1 kV. Drops of 3 µl of each protein sample were directly deposited on silicon wafers (Ted Pella Inc., Reading, CA, USA) for 1 min, excess blotted with Whatman filter paper number 1 (GE Healthcare, Piscataway, NJ, USA), air dried, and observed without coating with a high resolution in-lens secondary electron detector. For each sample, representative images of different fields were captured at (magnifications (from 120,000x to 200,000x).

2.5 Cell culture and flow cytometry

$CXCR4^+$ cervical, colorectal and pancreatic cancer cell lines were used to study the performance of the recombinant proteins in vitro (HeLa ATCC-CCL-2, SW1417 ATCC-CCL-238 and Panc-1 ATCC-CCL-1469). HeLa cells were maintained in Eagle's Minimum Essential Medium (Gibco®, Rockville, MD, USA), whereas SW1417 and Panc-1 in Dulbecco's Modified Eagle's Medium (Gibco®). All of them were supplemented with 10

% foetal bovine serum (Gibco®) and incubated in a humidified atmosphere at 37 ºC and 5 % of CO_2 (at 10 % for SW1417 cells).

In order to monitor protein internalization, HeLa cells were cultured on 24-well plates at $3{\cdot}10^4$ cells/well for 24 h until reaching 70 % confluence. Proteins were incubated for 1 h at different concentrations (100, 500 and 1,000 nM) in presence of OptiPRO™ SFM supplemented with L-glutamine. Additionally, specific internalization through CXCR4 receptor was proved adding a specific antagonist, AMD3100 [31, 32], which is expected to inhibit the interaction with T22. This chemical inhibitor was added 1 h prior protein incubation at a ratio of 1:10. Furthermore, kinetics of the internalization was performed at a concentration of 1 µM, after different periods of incubation (0, 20, 30, 60, 120, and 240 min). After protein exposure, cells were detached using 1 mg/ml Trypsin-EDTA (Gibco®) for 15 min at 37 ºC, a harsh protocol designed to remove externally attached protein [33]. The obtained samples were analyzed by a FACS-Canto system (Becton Dickinson, Franklin Lakes, NJ, USA) using a 15 mW air-cooled argon ion laser at 488 nm excitation. Experiments were performed in duplicate.

2.6 Confocal laser scanning microscopy

For confocal microscopy HeLa cells were grown on Mat-Tek plates (MatTek Corporation, Ashland, MA, USA). Upon exposure to the materials cell nuclei were labelled with 5 µg/ml Hoechst 33342 (ThermoFischer, Waltham, MA, USA) and the plasma membrane with 2.5 µg/ml CellMask™ Deep Red (ThermoFischer) for 10 min at room temperature. Cells were then washed in PBS buffer (Sigma-Aldrich, Steinheim, Germany). The confocal images of the HeLa cells were collected on an inverted TCS SP5 Leica Spectral confocal microscope (Leica Microsystems, Wetzlar, Germany) using 63x (1.4 NA) oil immersion objective lenses. Excitation was reached via a 405 nm blue diode laser (nucleic acids), 488 nm line of an argon ion laser (nanoparticles) and 633 nm line of a HeNe laser (Cell membrane). Optimized emission detection bandwidths were configured to avoid inter-channel crosstalk and multitrack sequential acquisition setting were used. The confocal pinhole was set to 1 Airy unit and z-stacks acquisition intervals were selected to satisfy Nyquist sampling criteria. Three-dimensional images

were processed using the Surpass Module in Imaris X64 v.7.2.1. software (Bitplane, Zürich, Switzerland).

2.7 Cell viability assays

The CellTiter-Glo® Luminescent Cell Viability Assay (Promega, Madison, WI, USA) was used to determine the cytotoxicity of T22-DITOX-H6, T22-PE24-H6, T22-DITOX-H6 F^- and T22-PE24-H6 F^- nanoparticles on HeLa, SW1417 $CXCR4^+$ or SW1417 $CXCR4^-$ cell lines. Cells were cultured in opaque-walled 96-well plates at 3,500 or 6,000 cells/well during 24 h at 37 ºC until reaching 70 % confluence. All protein incubations were performed in the corresponding medium according to the cell line used. Inhibition of cell death was analysed by adding AMD3100, a chemical antagonist of CXCR4 [34, 35], at a ratio of 1:10, 1 h prior to protein incubation. T22-GFP-H6, a non-functional T22-bearing protein [36] was also used as a competitor of T22-empowered toxins at a final concentration of 2 µM. After protein incubation, a single reagent provided by the manufacturer was added to cultured cells, which prompted lysis and generated a luminescent signal proportional to the amount of ATP present in the sample. The ATP generated is directly related to the quantity of living cells that remain in the well. Then, plates were measured in a conventional luminometer, Victor3 (Perkin Elmer, Waltham, MA, USA). Viability of Panc-1 cells, that overexpress luciferase, was determined with an alternative non fluorescence kit (EZ4U) under the same experimental conditions. The cell viability experiments were performed in triplicate.

2.8 Biodistribution, pharmacokinetics and apoptotic induction analyses in $CXCR4^+$ colorectal cancer mouse model after single dose administration of nanoparticles

All *in vivo* experiments were approved by the institutional animal Ethics Committee of Hospital Sant Pau. We used 5 week-old female Swiss Nu/Nu mice, weighing 18-20 g (Charles River, L'Abresle, France), maintained in specific pathogen-free conditions. To generate the subcutaneous (SC) mouse model, we implanted subcutaneously 10 mg of the patient-derived M5 colorectal (CCR) tumor tissue from donor animals in the mouse subcutis. At day 15, when tumors reached approximately 500 mm^3, mice received 50

µg single i.v. bolus of T22-DITOX-H6* (n = 3) or 300 µg single i.v. bolus of T22-PE24-H6* (n = 3) in $NaCO_3H$.NaCl, pH=8 buffer. Control animals received the same buffer (n = 3) or 0.25 µg of free ATTO 488 (n=2). At 5, 24 and 48 h mice were euthanized and subcutaneous tumors and organs (brain, lung, liver, kidney and heart) were collected. Biodistribution of ATTO-labelled nanoparticles in tumor and non-tumor organs was determined by measuring the emitted fluorescence in *ex vivo* tissue sections (3 mm thick) using the IVIS® Spectrum (Perkin Elmer, Santa Clara, CA, USA) platform. The fluorescent signal (FLI), which correlates to the amount of administered protein accumulated in each tissue, was first digitalized, displayed as a pseudocolor overlay, and expressed as radiant efficiency [(p/sec/cm2/sr)/µW/cm2]. The FLI values were calculated subtracting FLI signal from experimental mice by FLI auto-fluorescence of control mice. Samples were first fixed with 4 % formaldehyde in PBS for 24 h to be embedded in paraffin for histopathological evaluation and apoptotic index analyses.

Pharmacokinetic analyses were performed after a 300 µg single i.v. bolus administration of T22-PE24-H6* in 12 Swiss nude mice, or after a 50 µg single bolus administration of T22-DITOX-H6* also in 12 animals. We sacrificed three mice per each time point, at 0, 1, 2, 5, 24 and 48 h after the administration and obtained approximately 1 ml of blood EDTA anticoagulated collection tubes. We measured the exact volume of plasma obtained and the fluorescent emission at each time point, and calculated the concentration of nanoparticle as referred to the fluorescence emitted and concentration of the administered dose.

Apoptotic induction analyses were performed in 4 µm sections of tumors and normal organs (liver, lung, spleen, heart, kidney and brain) stained with hematoxylin and eosin (H&E), which were histopathologically analyzed by two independent observers. Apoptotic induction was evaluated by both, the presence of cell death bodies in H&E stained and Hoechst stained tumor slices. Triton X-100 (0.5 %) permeabilized sections were then stained with Hoechst 33258 (Sigma-Aldrich) diluted, 1:5,000 in PBS, for 1 h, rinsed with water, mounted and analyzed under fluorescence microscope (λex=334 nm/λem=465 nm). The number of apoptotic cell bodies was quantified by recording the number of condensed and/or defragmented nuclei per 10 high-power fields

(magnification 400x), in blinded samples evaluated by two independent researchers, using CellΛB s

2.9. Antitumor effect in a CXCR4+ CRC model after nanoparticle repeated dose administration

To generate the $CXCR4^+$ colorectal xenograft mouse models, we used the patient-derived M5 colorectal tumor tissue. Ten mg fragments obtained from donor animals were implanted in the subcutis of Swiss nu/nu mice to generate subcutaneous (SC) tumors as described above (n=9). Once tumors reached approximately 120 mm^3, mice were randomized in Control, T22-PE24-H6 and T22-DITOX-H6 groups and received intravenous doses of T22-PE24-H6 or T22-DITOX-H6, both at a repeated dose regime of 10 µg, 3 times a week, per 8 doses. The control group received buffer using the same administration schedule. Mouse body weight was registered over the experimental period 3 times a week. Seventeen days after the initiation of nanoparticle administration, mice were euthanized and the subcutaneous tumors were taken to measure their final tumor volume and to count the number of apoptotic figures in 5 high-power fields (magnification 400x), of H&E stained tumor sections as described above.

2.10 Statistical analysis

The specificity of nanoparticle-promoted cell death and the pairwise data comparisons were checked with a one-way ANOVA and Tukey's tests, respectively. Pairwise divergences of internalization and cell death were evaluated using Student's t tests, whereas Mann–Whitney U tests were used to pairwise comparisons of the number of apoptotic bodies. Differences between groups were considered significant at $p< 0.05$ and differences between relevant data are indicated by letters or as ¥ for $0.01 <p< 0.05$ and § for $p< 0.01$ in the Figures. All statistical analyses were performed using SPSS version 11.0 package (IBM, NY, USA), and values were expressed as mean ± standard error of the mean (SEM).

3 Results

Active fragments of the diphtheria toxin (DITOX) and the *Pseudomonas aeruginosa* exotoxin (PE24) were produced in *Escherichia coli* as the modular fusion proteins T22-DITOX-H6 and T22-PE24-H6 (Figure 1 A, B), intended to induce targeted cell death through the activity of the catalytic fragments of the protein drug (Figure 1C). The cationic peptide T22, placed at the amino terminus of the whole construct and cooperating with carboxy terminal histidines, promotes both oligomerization into regular nanoparticles [37] and binding to the cell-surface chemokine receptor CXCR4 (overexpressed in many aggressive human cancers [38-41]). In this way, it has been proved efficient in endorsing the endosomal penetration of payload GFP and IRFP into $CXCR4^{+}$ cancer stem cells [23]. Then, T22-DITOX-H6 spontaneously self-assembled into 38 and 90 nm-nanoparticles (Pdi= 0.25±0.01 nm) and T22-PE24-H6 into ~60 nm-nanoparticles (Pdi= 0.22±0.01, Figure 2A), always within the size range considered as optimal for efficient cell uptake [22, 42, 43]. A secondary population of protein material was observed in the case of T22-PE24-H6, being always minority. Nanoparticles were effectively disassembled by 0.1 % SDS, resulting in monodisperse building blocks peaking at ~6 nm (Pdi= 0.60±0.01 and 0.30±0.07 respectively), compatible with the expected size of the monomeric protein. However, both protein nanoparticles were fully stable in several physiological buffers in medium term incubation and also when exposed to high salt content buffer (up to 1 M NaCl, not shown), what prompted us expecting high stability *in vivo*. In addition, nanoparticles were found stable after one-year storage at -80ºC and upon repeated cycles of freezing and thawing (not shown). The assembled proteins appeared as toroid materials (Figure 2B), with ultrastructural morphometry (round shape and clear size populations) that confirmed the size range observed by DLS. The same regular architecture had been previously described for the related T22-GFP-H6 construct, in which the GFP-based sub-units (with a molecular size similar to that of T22-DITOX-H6 and T22-PE24-H6) organized in toroid entities, whose organization has been modelled *in silico* [44] and confirmed by sophisticated analytical methods such as SAXS or high resolution electron microscopy imaging techniques [45].

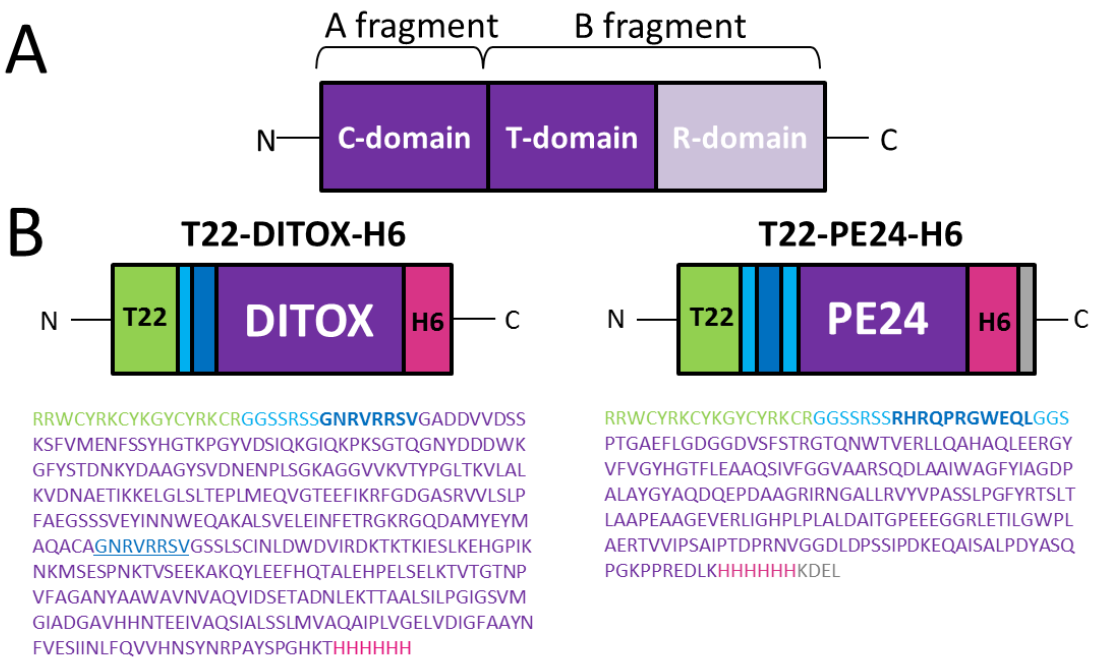

Figure 1. A. Native structure of A-B toxins such as diphtheria toxin (*Corynebacterium diphtheriae*) or exotoxin A (*Pseudomonas aeruginosa*). The native toxin is divided in two fragments (A and B). Fragment A includes the catalytic domain (C-domain), whereas the fragment B comprises the translocation and the receptor binding domain

(T- and R-domain). The selected domains for the construction of the recombinant nanoparticles are coloured in dark purple (T22-PE24-H6 construct does not include the T-domain). B. Modular organization of T22-DITOX-H6 and T22-PE24-H6, in which T22 acts as both CXCR4 ligand and as an architectonic tag. Functional segments are intersected by linker regions (light blue) and furin-cleavage sites (dark blue, boldface). A natural furin-cleavage site also occurs within DITOX (dark blue, underlined), that separates the amino terminal catalytic domain from the carboxy terminal translocation domain. A KDEL peptide has been incorporated neighboring the H6 region in T22-PE24-H6. Box sizes are only indicative. Two additional proteins, namely T22-DITOX-H6 F^- and T22-PE24-H6 F^- were constructed for comparative purposes, precisely lacking the engineered furin cleavage sites (boldface dark blue regions). C. Expected pathway for the cytotoxicity of T22-DITOX-H6 and T22-PE24-H6 nanoparticles over $CXCR4^+$ target cells, upon intracellular furin-mediated release of protein domains useful for biodistribution and cell penetration steps but irrelevant for cell killing.

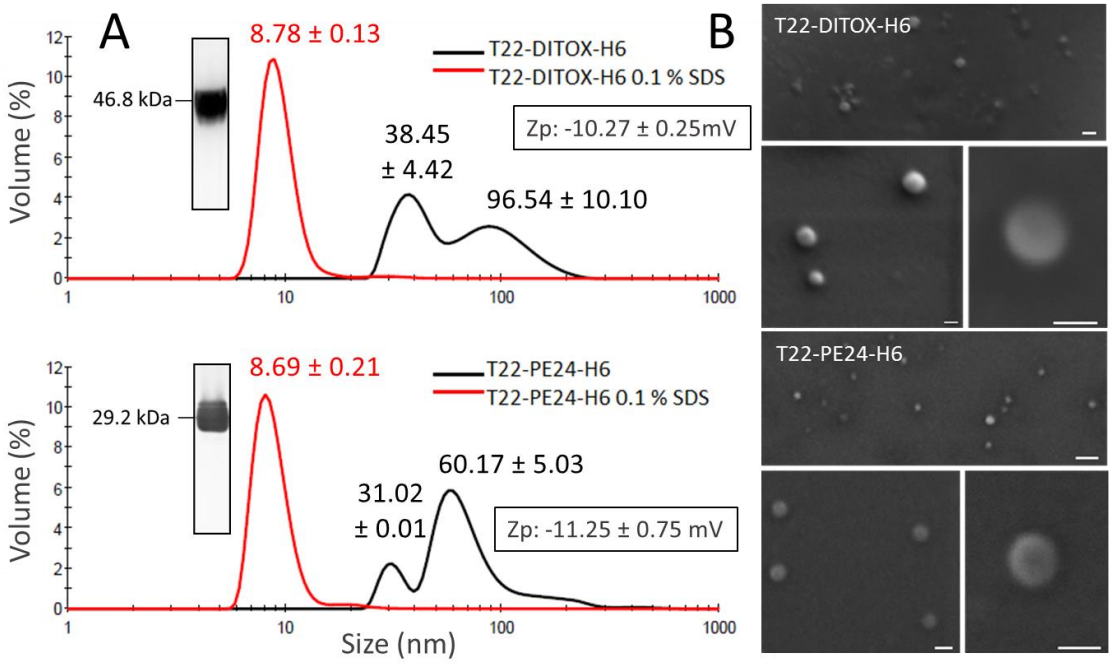

Figure 2. Nanoarchitecture of toxin-based proteins. A. Size and SDS-mediated disassembling of T22-DITOX-H6 and T22-PE24-H6 nanoparticles determined by DLS. Values of peak sizes (mode) are indicated in bold (in nm, ± SEM). Z-potential (Zp) values of the nanoparticles are also indicated. The molecular mass of proteins upon purification is shown by Western Blot upon PAGE-SDS. B. FESEM examination of purified T22-DITOX-H6 and T22-PE24-H6 materials. Bars indicate 50 nm.

Purified T22-DITOX-H6 and T22-PE24-H6 nanoparticles were tested for internalization into cultured $CXCR4^+$ cells, upon chemically labelling with the fluorescent dye ATTO 488 (tagged with *, Figure 3A). Both kinds of labelled nanoparticles (Figure 3A)

penetrated target HeLa cells in a dose-dependent manner (Figure 3B) and accumulated intracellularly with a kinetics characteristic of receptor-mediated uptake (with a faster slope in the case of T22-PE24-H6*, Figure 3C). The CXCR4 specificity of the penetration was confirmed through its inhibition by the CXCR4 antagonist AMD3100 [34] (Figure 3D). Internalized nanoparticles were observed as engulfed into endosomes, especially in cytoplasm areas close to the cell membrane, but they tended to be visualized as membrane-free entities when approaching the perinuclear regions (Figure 3E), suggesting important endosomal escape. No cell-attached extracellular fluorescence was observed in any case.

Once the internalization was assessed, we tested if the furin cleavage sites introduced in the constructs to release the toxin segments from the building blocks were active in the oligomers. The expected intracellular hydrolysis should enhance the cytotoxic properties of the toxin domains, which would then benefit from lower load of superfluous protein sequences. For that, we explored the sensitivity of the multiple cleavage sites in the construct T22-DITOX-H6 that would offer, upon intracellular digestion, fully distinguishable protein fragments. Unlike the extracellular protein that appears as one single protein species (Figure 2A and 3A), the His tag immunodetection of the cell-engulfed protein showed the protein as digested by different alternative sites, matching the molecular weight of the expected products for each furin cleavage site. In particular, the release of the T22 peptide through the de novo incorporated cleavage site was proved *in vivo* in cell-internalized protein by the shift from the 48.65 KDa full-length protein to the 44.21 KDa fragment, analyzing cell extracts upon exposure to the nanoparticles for 24 h (Figure 4A). The rest of fragments corresponded to the progressive digestion intermediates that still kept the carboxy terminal tag, by which the protein is immunodetected. The natural cleavage at the internal furin site, which releases the catalytic domain from the translocation domain, is also proved by the occurrence of the major 20.60 KDa segment. Therefore, the catalytic segment alone is expected to occur inside the target cells, among other biologically active versions, at reasonable amounts.

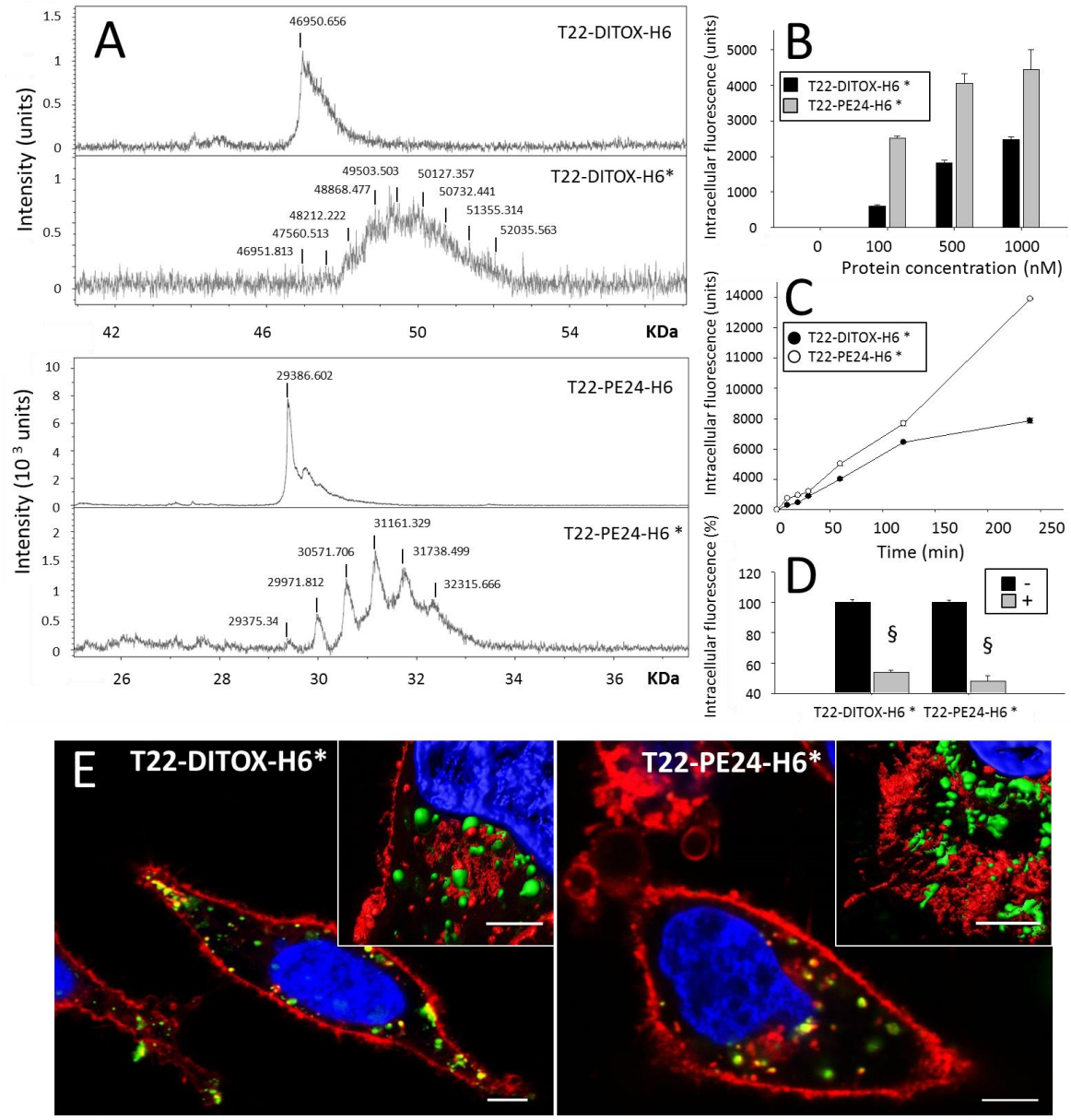

Figure 3. Internalization of toxin-based nanoparticles in CXCR4⁺ cells. A. Mass spectroscopy of pure unlabeled and ATTO-labelled (*) T22-DITOX-H6 and T22-PE24-H6 proteins. B. Dose-dependent uptake of T22-DITOX-H6* and T22-PE24-H6* nanoparticles in CXCR4⁺ HeLa cells upon 1 h of exposure. C. Time course kinetics of cell internalization of T22-DITOX-H6* and T22-PE24-H6* nanoparticles (1 µM) in CXCR4⁺ HeLa cells. Note the short error bars in the plot. D. Protein (100 nM) uptake inhibition by the CXCR4 antagonist AMD3100 (+) upon 1 h of exposure. Significant differences between relevant data pairs are indicated as § for $p < 0.01$. All A, B and C data are presented as mean ± SEM (n = 2). E. Confocal microscopy of HeLa cells exposed for 5 h to T22-DITOX-H6* and T22-PE24-H6* nanoparticles (1 µM). The Cell Mask membrane staining (red) was added together with nanoparticles to observe the endosomal membrane. Nanoparticles are visualized in green and nuclear regions in blue. The yellow spots indicate merging of red and green signals. In the insets, 3D Imaris reconstructions of confocal stacks. Bars indicate 5 µm.

When exploring the cytotoxic effects, both T22-DITOX-H6 and T22-PE24-H6 were effective in killing cultured HeLa cells, with low IC50 values (0.78 nM and 0.99 nM respectively, not shown). The cytotoxic effect was clearly detectable in several CXCR4-expressing cell lines, including SW1417 $CXCR4^+$ but not in the isogenic SW1417 $CXCR4^-$ line (Figure 4B, left). Cytotoxicity was mostly abolished by AMD3100 and by the T22-displaying biologically inner protein T22-GFP-H6 (Figure 4B, right), thus confirming again the specificity of the entrance of the nanoparticles, the intracellular nature of the nanoparticle-mediated toxicity and the expected CXCR4 receptor mediation in cell killing. Besides, it has been observed a reversion effect of T22-DITOX-H6 (90 %) when adding chloroquine, which inhibits endosomal acidification (not shown). This fact confirms that the mechanism of action is pH-dependent as described above (Figure 1). In this context, we also evaluated the relevance of the removal of accessory protein segments (mediated by furin) on the cytotoxicity of the nanoparticles. For that, versions of T22-DITOX-H6 and T22-PE24-H6 without the engineered cleavage sites (labelled as F^-) were constructed and tested for biological activity. The comparative analyses of HeLa cell death mediated by these proteins revealed a dramatic drop of cytotoxicity in T22-DITOX-H6 F^- and T22-PE24-H6 F^- nanoparticles compared to the original materials (Figure 4 C). On the other hand, the differential CXCR4 expression in the isogenic SW1417 cells was fully assessed by immunocytochemistry and Western blot (Figure 4 D,E). Interestingly, the capacity of T22-DITOX-H6 and T22-PE24-H6 to promote cell death was not lost after one-year storage at -80ºC and also upon four cycles of freezing and thawing (not shown).

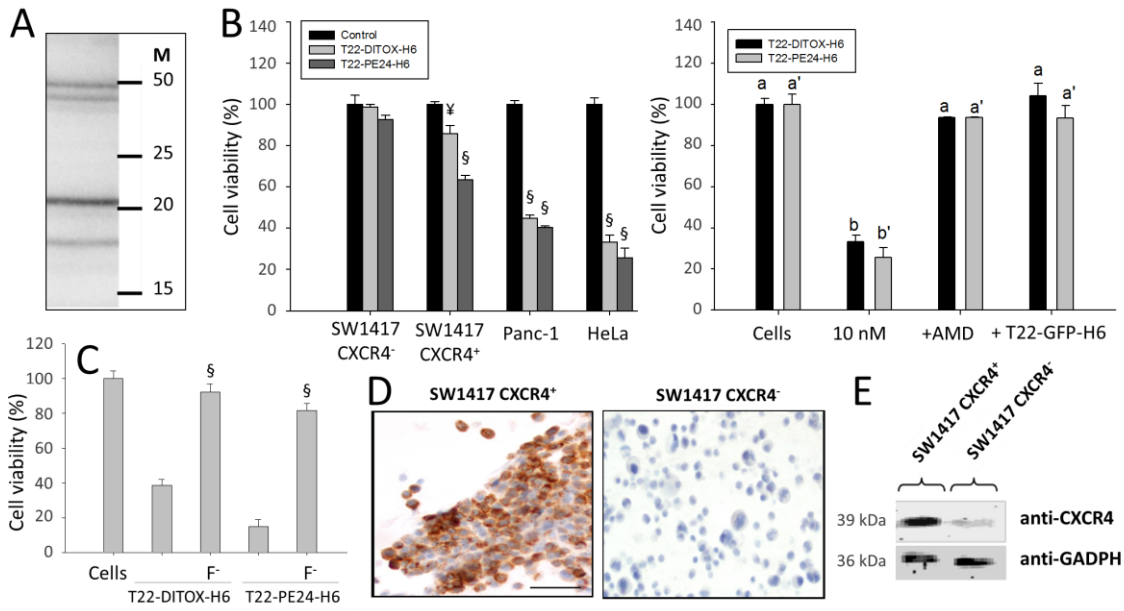

Figure 4. Specific cytotoxicity of toxin-based nanoparticles in CXCR4⁺ cells. A. Detection of intracellular T22-DITOX-H6 by Western blot analysis of HeLa cell extracts, after exposure of the cell cultures to nanoparticles (1 µM protein) for 24 h. **M** indicates the migration of molecular weight markers. B. Left: Cell death induced by T22-DITOX-H6 and T22-PE24-H6 nanoparticles (10 nM) over a SW1417 CXCR4⁻ cell line and different CXCR4⁺ cell lines (including an isogenic, CXCR4⁺ SW1417 version), 48 h after exposure (72 h for SW1417 cell line). Significant differences between relevant data pairs are indicated as ¥ $0.01 < p < 0.05$ and § $p < 0.01$. Right: inhibition of HeLa cell death (induced by 10 nM of protein nanoparticles) by either the CXCR4 antagonist AMD3100 or by 2 µM protein T22-GFP-H6. Significant differences between relevant data are indicated as a change in the letter, from "a" to "b". All the significant results were $p < 0.01$. All data are presented as mean ± SEM (n = 3). C. HeLa cell death promoted by T22-DITOX-H6 F⁻ and by T22-PE24-H6 F⁻, compared to the related T22-DITOX-H6 and by T22-PE24-H6 respectively. Cells were exposed to 10 nM of each protein for 48 h. Data and statistics are as in panel B. D. Immunocytochemistry staining showing the lack of CXCR4 expression in the isogenic SW1417 CXCR4⁻ cells as compared with the high CXCR4 expression in SW1417 CXCR4⁺ cells. Bar indicates 50 µm. E. Differential CXCR4 protein expression in these cells assessed by an immunoblotting assay. Glyceraldehyde-3-phosphate dehydrogenase (GADPH) was used as protein loading control.

Due to the high CXCR4⁺ specific cytotoxicity observed in cell culture, we next tested the performance of the toxin-based materials *in vivo* using a CXCR4-linked disease model. For that, we explored the biodistribution, antitumor activity and potential side

toxicity of both T22-DITOX-H6* and T22-PE24-H6* nanoparticles in a CXCR4 overexpressing subcutaneous colorectal cancer model. As expected, after a single dose i.v. administration the protein materials accumulated in tumor in the studied time range (Figure 5). Other organs such as brain, lung or heart were completely free of fluorescence. However, significant levels of emission associated to both nanoparticles were found in liver and kidney. To discard that significant amounts of ATTO might had been released from the nanoparticles during circulation in blood and generate artefacts in the biodistribution analysis, we evaluated the stability of the dye in T22-DITOX-H6* nanoparticles incubated in commercial serum. At 48 h, only a very minor fraction of fluorescence was released from nanoparticles (5 %, Supplementary Figure 1 A). In addition, the administration of free ATTO did not resulted in detectable accumulation in tumor (Supplementary Figure 1 B), and the absence of dye signal in major organs was indicative of a fast urine secretion (as expected for a small molecule of 981 Da). These data fully supported the biodistribution of labelled nanoparticles shown in Figure 5.

The presence of nanoparticles in liver was observed as worthy of a deeper analysis, since hepatic occurrence and damage is a severe concern in conventional and innovative cancer therapies, even in nanoconjugates or antibody-based drugs that show tissue-specific targeting [46-51]. Then, since it would be of crucial interest to discriminate between mere occurrence of fluorescence and toxin-induced damage in these organs, we comparatively investigated cell damage in tumor, liver and kidney. In this regard, we observed a high level of apoptosis induced by both nanoparticles in tumoral tissue, what was especially intense in T22-PE24-H6*-treated animals at 48 h post administration (Figure 6). In contrast, apoptosis was undetectable in liver or kidney (Figure 6), and most of the hepatic tissues were histologically normal except for a few and scattered small inflammation foci (Figure 6) that can be attributed to non-specific extracellular retention of the drug in off-target tissues. This alteration was resolved after 72 h returning to normal histology. Probably, the intracellular activation of the toxins promoted by the furin-mediated release of accessory peptides (Figure 4) does not occur in hepatic tissue, which does not overexpress CXCR4.

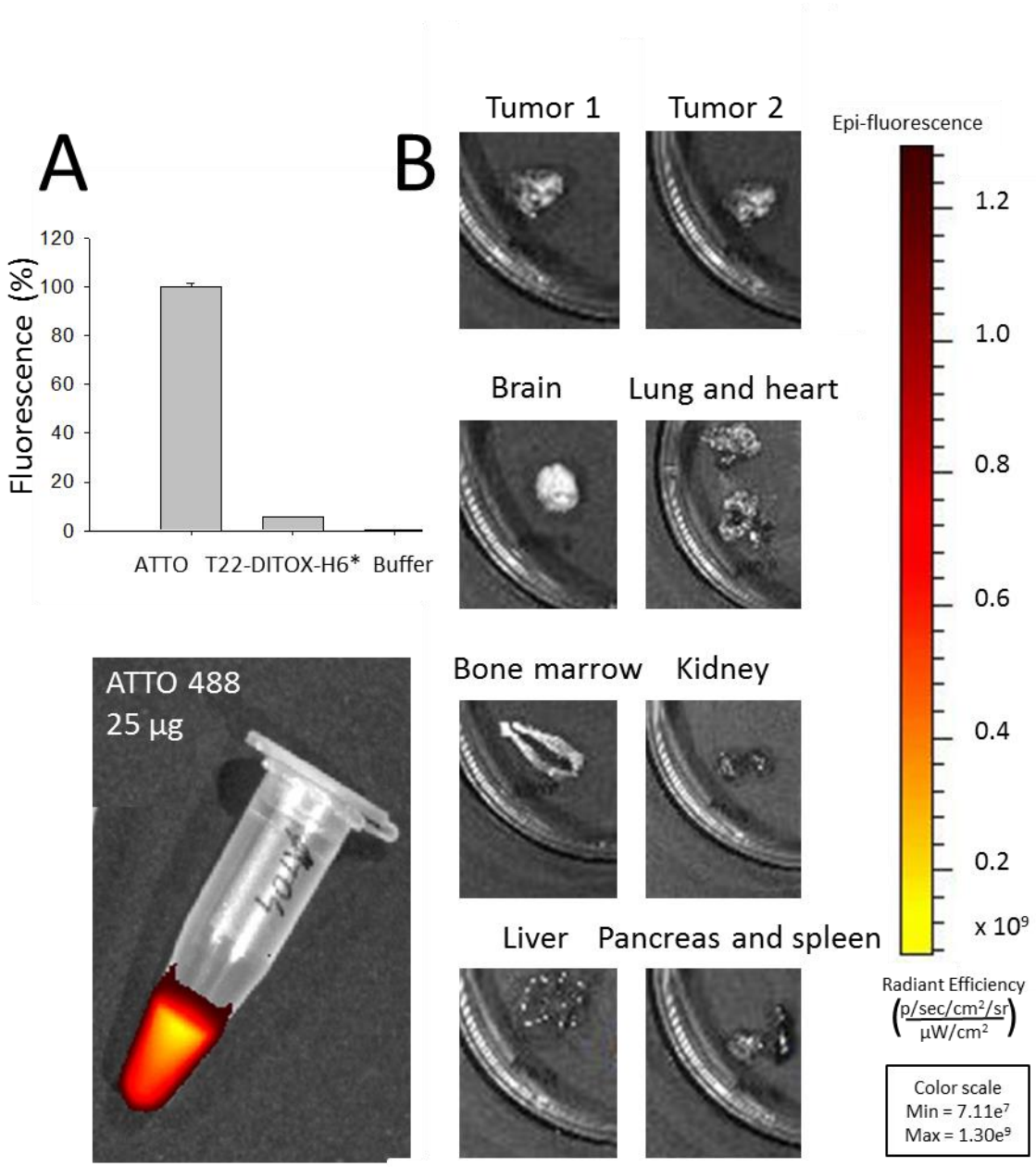

Supplementary Figure 1. Robustness of conjugated ATTO in the biodistribution analysis. A. ATTO released from T22-DITOX-H6* nanoparticles upon *in vitro* incubation with commercial sera for 48 h at 37 ºC. Data is obtained by analyzing the dialysis buffer and it is referred to dialyzed free ATTO (100 %). Data are presented as mean ± SEM, n=4. B. Biodistribution of injected free ATTO 5 h after injection. The ATTO sample before inoculation is shown at the bottom. Tumor 1 and 2 refer to two different experiments with independent mice. The rest of organs were extracted from animal number 1.

To discard that ATTO might have a positive contribution in the cytotoxicity of the materials in tumor after single dose administration we checked local apoptosis in animals treated with the non-labelled protein versions T22-DITOX-H6 and T22-PE24-H6. This was done at the times, among those tested, showing the highest potency (24 and 48 h respectively). As observed, local apoptosis was still present (Figure 6) at values even higher than those induced by the labelled protein versions. This result was indicative that the observed antitumoral effect was intrinsically associated to the protein material. Then, data supported the notion that in spite of the occurrence of the protein drug in liver and kidney, this did not translate in a relevant uptake of any of the two nanoparticles in the parenchyma of these tissues. Our observations suggest that both labelled protein drugs underwent transient circulation through the fenestrated hepatic sinusoids and renal glomeruli despite their nanometric size (in contrast to other normal tissues) as reported for other nanoparticles [52]. Moreover, their lack of toxicity in kidney or liver suggest their inability to internalize into the parenchymal cells in these organs because of their negligible CXCR4 expression, in comparison for instance to spleen or bone marrow which despite showing low nanoparticle accumulation express CXCR4 [53]. This is a finding similar to that reported for CXCR4-targeted imaging agents [54]. Then, both T22-DITOX-H6 and T22-PE24-H6 appear to have a therapeutic index high enough to validate (i) their potential use for the treatment of $CXCR4^+$ tumors but more importantly, (ii) the wide applicability of the transversal concept supporting the self-assembling self-driving protein drugs based on chemically homogenous building blocks.

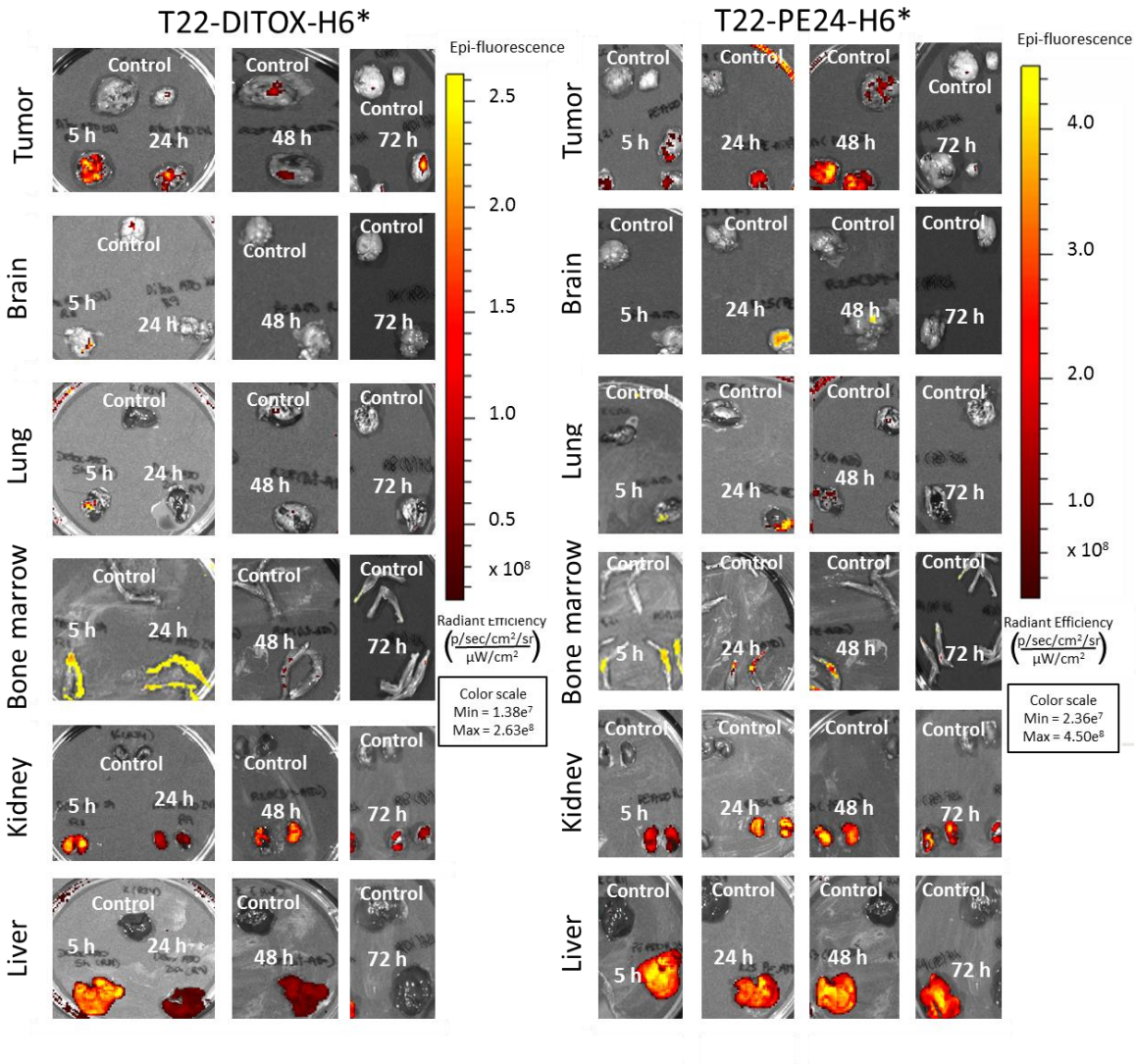

Figure 5. Biodistribution kinetics of T22-DITOX-H6* and T22-PE24-H6* nanoparticles in a CXCR4⁺ colorectal cancer mouse model. *Ex vivo* fluorescence emitted by subcutaneous tumor and relevant organs in buffer-administered (control) and T22-DITOX-H6*- and T22-PE24-H6*-treated mice at 5, 24, 48 and 72 h after 50 µg or 300 µg single dose i.v. administration. Emission scales are shown as radiant efficiency units (see methods section).

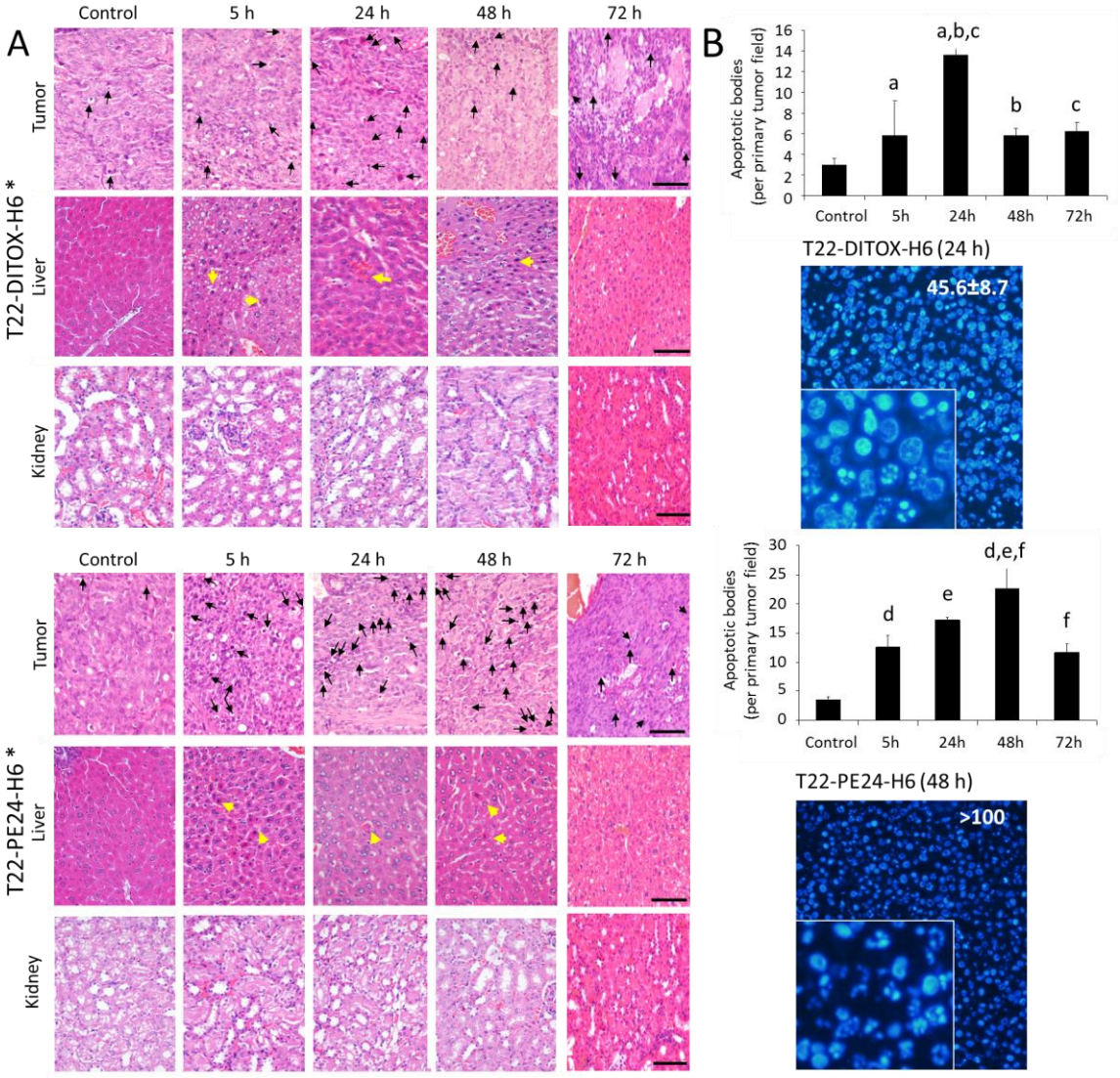

Figure 6. Local induction of apoptosis in tumor by ATTO-labelled and unlabeled T22-DITOX-H6 (50 µg) and T22-PE24-H6 (300 µg) nanoparticles. A. Representative H&E staining of subcutaneous tumors showing apoptotic figures (black arrows). No significant apoptosis was detected in liver tissue at the studied times. Few and small inflammation foci in this organ were observed and are indicated by yellow arrows, which were resolved at 72 h, returning to histologically normal parenchyma. Note the absence of histological alterations in kidneys. Bar: 50 µm. **B.** Number of apoptotic cell bodies in H&E tumor slices per ten high-power fields (400× magnification) are plotted for each nanoparticle. For the experimental times showing higher number of apoptotic lesions we also show representative Hoechst staining of subcutaneous tumors in animals treated with unlabeled protein versions, at different magnifications. All data are presented as mean ± SEM (n = 3). Statistical significance: $^{a}p=0.008$; $^{b}p=0.027$; $^{c}p=0.010$; ^{d,e,f} p= 0.001.

In order to evaluate further the therapeutic potential of the engineered toxins and the concepts that support the design of toxin-based nanoparticles we also assessed the pharmacokinetics in blood mouse samples after a single dose of 50 μg for T22-DITOX-H6* or 300 μg for T22-PE24-H6*. This was done through registering their fluorescence emission at 0, 1, 2, 5, 24 and 48 h after administration. We observed a biphasic decline in plasma concentration from Cmax, with a fast nanoparticle biodistribution limited to the plasma compartment for both tested proteins (Vd=3.9 ml T22-PE-H6* and Vd=3.2 ml for T22-DITOX-H6*). This fast biodistribution was followed by a second and slow elimination phase, with a half-life of t1/2 = 30 h for both nanoparticles (Figure 7 A). This kinetic behavior is similar to the one we previously reported for pharmacologically inactive protein nanoparticles [23], and also similar to that described for antibody-drug conjugates or large nanometric size therapeutic proteins, which show a comportment similar to the unconjugated antibody [55].

In a step further, we assessed the antitumor effect of each nanoparticle in a $CXCR4^+$ subcutaneous CRC mouse model after repeated dose administration. After a dosage schedule of 10 μg of T22-DITOX-H6, three times a week, per 8 doses, we observed at the end of the experiment a 5.8-fold reduction in tumor volume, as compared to buffer-treated mice ($p=0.05$). This was associated with a 3.0-fold increase in apoptoptic figures in tumor tissue ($p<0.001$) (Figure 7 B), with no significant differences in body weight between toxin-treated and control groups (Figure 7 C). Similarly, and after a dosage schedule in mice of 10 μg of T22-PE24-H6, three times a week, per 8 doses, we observed at the end of the experiment a 2.3-fold reduction in tumor volume, as compared to buffer-treated mice ($p=0.034$), associated with a 3.8-fold increase in the number of apoptotic figures in tumor tissue ($p=0.001$) (Figure 7 B). Again, no significant differences in body weight between experimental and control groups were observed (Figure 7 C).

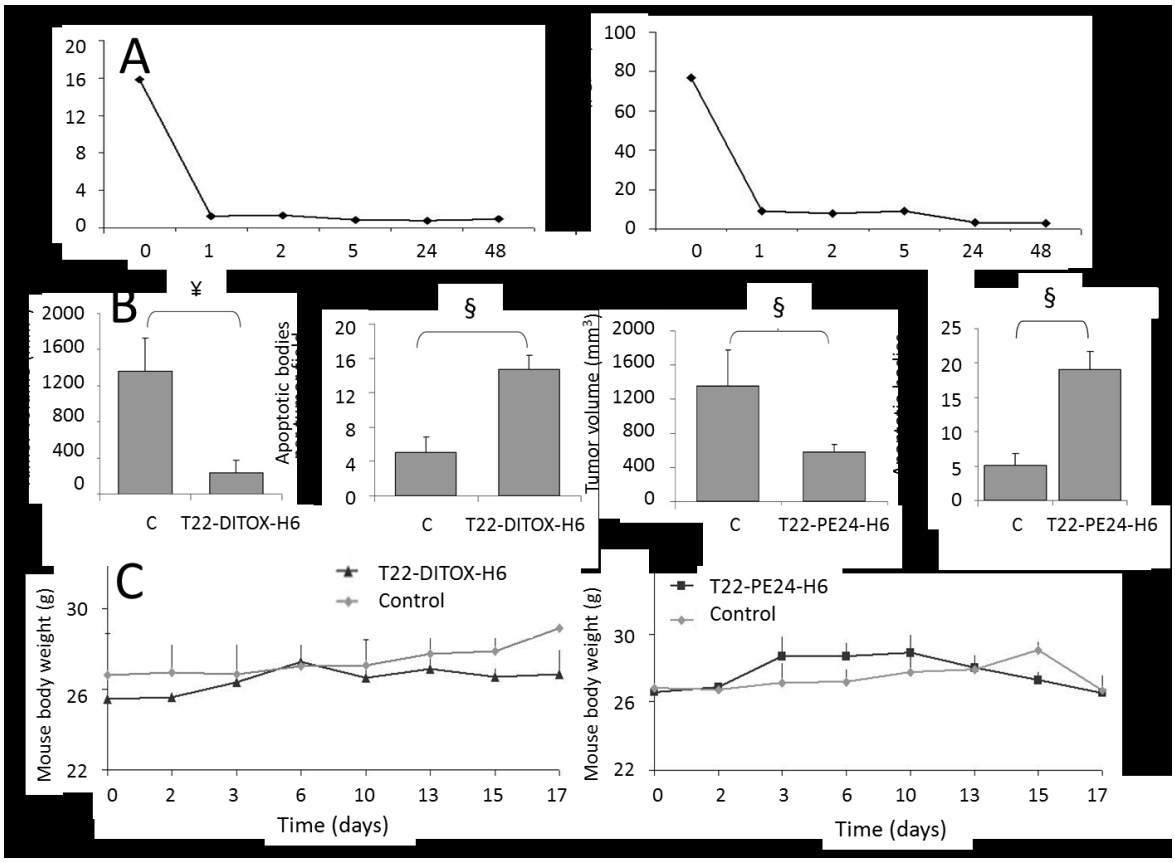

Figure 7. Pharmacokinetics, antitumoral effect and mouse body weight after T22-DITOX-H6 and T22-PE24-H6 administration. A. Pharmacokinetics of T22-DITOX-H6* and T22-PE24-H6* after a 50 µg or 300 µg intravenous bolus administration respectively. Fluorescence was recorded in plasma obtained after blood centrifugation at time 0, 1, 2, 5, 24 and 48 h (n=3 per time point). B. Antitumor effect of T22-DITOX-H6 and T22-PE24-H6 measured by the analysis of tumor volume and number of apoptotic bodies at the end of the experiment, after repeated dose administration for each nanoparticle (10 µg, three times a week, × 8 doses). C. Evolution of mouse body weight after the described repeated dose regime for the protein nanoparticles. Statistics are ¥ for 0.01 <p< 0.05 and § for p< 0.01. All data are presented as mean ± SEM, n=3.

4 Discussion

This set of data is in the line of new nanomedical concepts in targeted drug delivery in which the drugs itself act, in addition to their therapeutic functionalities, as self-assembled and self-delivered entities [18]. Conveniently engineered, the protein drugs developed here have been successfully produced and purified in bacteria, and self-organize as toroid nanoparticles of 30-90 nm (Figure 2). In this form, they penetrate $CXCR4^+$ target cells (Figure 3) and promote receptor specific cell killing both *in vitro*

(Figure 4) and *in vivo* (Figure 6), resulting in significant programmed cell death induction and in destruction of tumoral tissue after single dose administration (Figure 6). Moreover, after repeated dose administration the nanostructured toxins increase apoptosis in tumor tissue associated with a significant reduction of tumor volume, with no alteration of mouse body weight (Figure 7). These data prove the realistic feasibility of the application of these nanostructured toxins in a true therapeutic context. In comparison with similar approaches to generate self-assembling peptidic drugs (as pro-apoptotic and antimicrobial agents) [24, 56], the concept explored here (i) does not use supporting irrelevant proteins such as GFP, thus minimizing the amount of bulk inactive material in the drug and enhancing nominal productivity in cell factories and (ii) allows the releasing of the active proteins in the cell cytoplasm by the controlled discharging of accessory protein segments that had been exploited for self-assembling of the building blocks and for the biodistribution and cell-targeted internalization of the nanoparticles. In this regard, the intrinsic cytotoxicity of the protein drugs is dramatically enhanced by the occurrence of the active domain free from siding accessory peptides (Figure 4). This is achieved by the appropriate incorporation of intracellular cleavage sites in the fusion protein that allow protein activation once in the right cell compartment and promotes the cytotoxic activity being executed solely by the minimal functional protein domain. As a generic concept, removing the vehicle in cell-targeted nanomedicines [18], would replace the otherwise promoted nanoconjugate strategies [57] through the design of new generations of chemically homogeneous nanoscale drugs. This would not only allow a heavy reduction of fabrication costs, but it will also minimize off-target drug effects, smoother regulatory constraints to drug approval and reduce the concerns about individual and environmental toxicity of inappropriate materials used as carriers. In this regard, other examples of self-assembling, self-delivered drugs are based on the combination of different types of molecules to achieve their function. Note the aggregation of VEGF siRNA, PolyMet (polymeric metmorfine), polyethylenimine, dicyandiamide, hyaluronic acid, DOTAP, cholesterol, DOTAP and a pegylated targeting ligand [19], or of EGCG, PEG, and herceptin or interferon α-2a [20] in self-delivered materials (summarized in [18]). The exceptional but technologically simple functional recruitment offered by proteins in single polypeptide chains [21] allows not only purifying the drug from

recombinant cell factories in a single step by fully standardized recombinant DNA technologies [9], but globally, it also conduces to the simple design of self-assembling nanoparticles that can be easily fabricated in promising endotoxin-free bacterial systems [58, 59].

5 Conclusions

We provide here data that fully supports an emerging ground-breaking concept in nanomedicine that is the generation of self-assembled, self-delivered drugs that act in absence of any external vehicle [18]. The approach presented here, based on modular recombinant proteins, allows the single-step biological production of nanostructured protein materials that exhibit intrinsic therapeutic properties and show an appropriate cell targeting and biodistribution upon systemic administration. This is linked to a specific biological impact (tumor tissue destruction leading to tumor shrinkage) at the local level, because of the cell targeting domains included in the nanoparticle. These functional stretches, useful for biodistribution and during the delivery process, are self-removed from the protein nanoparticles once they have reached the target cell compartment. Then, the cytotoxic protein domain acts very efficiently free from any accessory protein segment. The design of self-organizing, cell-targeted protein drugs at the nanoscale level represents a step forward towards chemically homogeneous nanomedicines that should allow to full discard additional, potentially deleterious carriers.

References

[1] Calvete JJ, Sanz L, Angulo Y, Lomonte B, Gutierrez JM. Venoms, venomics, antivenomics. FEBS letters 2009;583:1736-43.

[2] Koh CY, Kini RM. From snake venom toxins to therapeutics--cardiovascular examples. Toxicon : official journal of the International Society on Toxinology 2012;59:497-506.

[3] Russo P, Del Bufalo A, Fini M. Deep sea as a source of novel-anticancer drugs: update on discovery and preclinical/clinical evaluation in a systems medicine perspective. EXCLI journal 2015;14:228-36.

[4] Livett BG, Gayler KR, Khalil Z. Drugs from the sea: conopeptides as potential therapeutics. Current medicinal chemistry 2004;11:1715-23.

[5] D'Incalci M, Simone M, Tavecchio M, Damia G, Garbi A, Erba E. New drugs from the sea. Journal of chemotherapy 2004;16 Suppl 4:86-9.

[6] Fox JW, Serrano SM. Approaching the golden age of natural product pharmaceuticals from venom libraries: an overview of toxins and toxin-derivatives currently involved in therapeutic or diagnostic applications. Current pharmaceutical design 2007;13:2927-34.

[7] Kotova S, Wong RM, Cameron RB. New and emerging therapeutic options for malignant pleural mesothelioma: review of early clinical trials. Cancer management and research 2015;7:51-63.

[8] Finnerup NB, Attal N, Haroutounian S, McNicol E, Baron R, Dworkin RH, et al. Pharmacotherapy for neuropathic pain in adults: a systematic review and meta-analysis. The Lancet Neurology 2015;14:162-73.

[9] Sanchez-Garcia L, Martin L, Mangues R, Ferrer-Miralles N, Vazquez E, Villaverde A. Recombinant pharmaceuticals from microbial cells: a 2015 update. Microbial cell factories 2016;15:33.

[10] Sarfo-Poku C, Eshun O, Lee KH. Medical application of scorpion venom to breast cancer: A mini-review. Toxicon : official journal of the International Society on Toxinology 2016;122:109-12.

[11] Chaisakul J, Hodgson WC, Kuruppu S, Prasongsook N. Effects of Animal Venoms and Toxins on Hallmarks of Cancer. Journal of Cancer 2016;7:1571-8.

[12] Zhan C, Li C, Wei X, Lu W, Lu W. Toxins and derivatives in molecular pharmaceutics: Drug delivery and targeted therapy. Advanced drug delivery reviews 2015;90:101-18.

[13] Bachran C, Leppla SH. Tumor Targeting and Drug Delivery by Anthrax Toxin. Toxins 2016;8.

[14] Li YM, Hall WA. Targeted toxins in brain tumor therapy. Toxins 2010;2:2645-62.

[15] Rainov NG, Soling A. Clinical studies with targeted toxins in malignant glioma. Reviews on recent clinical trials 2006;1:119-31.

[16] Elsaesser A, Howard CV. Toxicology of nanoparticles. Advanced drug delivery reviews 2012;64:129-37.

[17] Haynes C. Editorial--analytical toxicology of nanoparticles. The Analyst 2014;139:868-9.

[18] Shen J, Wolfram J, Ferrari M, Shen H. Taking the vehicle out of drug delivery. Materials today 2017;20:95-7.

[19] Zhao Y, Wang W, Guo S, Wang Y, Miao L, Xiong Y, et al. PolyMetformin combines carrier and anticancer activities for in vivo siRNA delivery. Nat Commun 2016;7:11822.

[20] Chung JE, Tan S, Gao SJ, Yongvongsoontorn N, Kim SH, Lee JH, et al. Self-assembled micellar nanocomplexes comprising green tea catechin derivatives and protein drugs for cancer therapy. Nature nanotechnology 2014;9:907-12.

[21] Vazquez E, Mangues R, Villaverde A. Functional recruitment for drug delivery through protein-based nanotechnologies. Nanomedicine 2016;11:1333-6.

[22] Duncan R, Gaspar R. Nanomedicine(s) under the microscope. Molecular pharmaceutics 2011;8:2101-41.

[23] Cespedes MV, Unzueta U, Tatkiewicz W, Sanchez-Chardi A, Conchillo-Sole O, Alamo P, et al. In vivo architectonic stability of fully de novo designed protein-only nanoparticles. ACS nano 2014;8:4166-76.

[24] Naroa Serna MVC, Laura Sánchez-García, Ugutz Unzueta, Rita Sala, Alejandro Sánchez-Chardi, Francisco Cortés, Neus Ferrer-Miralles, Ramón Mangues, Esther Vázquez and Antonio Villaverde. Peptide-Based Nanostructured Materials with Intrinsic Proapoptotic Activities in CXCR4+ Solid Tumors. Advanced Functional Materials 2017.

[25] Collier RJ. Understanding the mode of action of diphtheria toxin: a perspective on progress during the 20th century. Toxicon : official journal of the International Society on Toxinology 2001;39:1793-803.

[26] Michalska M, Wolf P. Pseudomonas Exotoxin A: optimized by evolution for effective killing. Frontiers in microbiology 2015;6:963.

[27] Seetharam S, Chaudhary VK, FitzGerald D, Pastan I. Increased cytotoxic activity of Pseudomonas exotoxin and two chimeric toxins ending in KDEL. The Journal of biological chemistry 1991;266:17376-81.

[28] Holmes RK. Biology and molecular epidemiology of diphtheria toxin and the tox gene. J Infect Dis 2000;181 Suppl 1:S156-67.

[29] Wong BY, Gregory SA, Dang NH. Denileukin diftitox as novel targeted therapy for lymphoid malignancies. Cancer investigation 2007;25:495-501.

[30] Bauss F, Lechmann M, Krippendorff BF, Staack R, Herting F, Festag M, et al. Characterization of a re-engineered, mesothelin-targeted Pseudomonas exotoxin fusion protein for lung cancer therapy. Molecular oncology 2016;10:1317-29.

[31] Kim HY, Hwang JY, Kim SW, Lee HJ, Yun HJ, Kim S, et al. The CXCR4 Antagonist AMD3100 Has Dual Effects on Survival and Proliferation of Myeloma Cells In Vitro. Cancer research and treatment : official journal of Korean Cancer Association 2010;42:225-34.

[32] Song JS, Kang CM, Kang HH, Yoon HK, Kim YK, Kim KH, et al. Inhibitory effect of CXC chemokine receptor 4 antagonist AMD3100 on bleomycin induced murine pulmonary fibrosis. Experimental & molecular medicine 2010;42:465-72.

[33] Richard JP, Melikov K, Vives E, Ramos C, Verbeure B, Gait MJ, et al. Cell-penetrating peptides. A reevaluation of the mechanism of cellular uptake. The Journal of biological chemistry 2003;278:585-90.

[34] Kim J, Connelly KL, Unterwald EM, Rawls SM. Chemokines and cocaine: CXCR4 receptor antagonist AMD3100 attenuates cocaine place preference and locomotor stimulation in rats. Brain, behavior, and immunity 2016.

[35] Jung YH, Lee DY, Cha W, Kim BH, Sung MW, Kim KH, et al. Antitumor effect of CXCR4 antagonist AMD3100 on the tumorigenic cell line of BHP10-3 papillary thyroid cancer cells. Head & neck 2016;38:1479-86.

[36] Unzueta U, Cespedes MV, Ferrer-Miralles N, Casanova I, Cedano J, Corchero JL, et al. Intracellular CXCR4(+) cell targeting with T22-empowered protein-only nanoparticles. International journal of nanomedicine 2012;7:4533-44.

[37] Unzueta U, Ferrer-Miralles N, Cedano J, Zikung X, Pesarrodona M, Saccardo P, et al. Non-amyloidogenic peptide tags for the regulatable self-assembling of protein-only nanoparticles. Biomaterials 2012;33:8714-22.

[38] Koshiba T, Hosotani R, Miyamoto Y, Ida J, Tsuji S, Nakajima S, et al. Expression of stromal cell-derived factor 1 and CXCR4 ligand receptor system in pancreatic cancer: a possible role for tumor progression. Clinical cancer research : an official journal of the American Association for Cancer Research 2000;6:3530-5.

[39] Kulbe H, Levinson NR, Balkwill F, Wilson JL. The chemokine network in cancer--much more than directing cell movement. The International journal of developmental biology 2004;48:489-96.

[40] Murakami T, Cardones AR, Hwang ST. Chemokine receptors and melanoma metastasis. Journal of dermatological science 2004;36:71-8.

[41] Barbieri F, Bajetto A, Florio T. Role of chemokine network in the development and progression of ovarian cancer: a potential novel pharmacological target. Journal of oncology 2010;2010:426956.

[42] Albanese A, Tang PS, Chan WC. The effect of nanoparticle size, shape, and surface chemistry on biological systems. Annual review of biomedical engineering 2012;14:1-16.

[43] Chithrani BD, Ghazani AA, Chan WC. Determining the size and shape dependence of gold nanoparticle uptake into mammalian cells. Nano letters 2006;6:662-8.

[44] Rueda F, Cespedes MV, Conchillo-Sole O, Sanchez-Chardi A, Seras-Franzoso J, Cubarsi R, et al. Bottom-Up Instructive Quality Control in the Biofabrication of Smart Protein Materials. Advanced materials 2015;27:7816-22.

[45] Pesarrodona M, Crosas E, Cubarsi R, Sanchez-Chardi A, Saccardo P, Unzueta U, et al. Intrinsic functional and architectonic heterogeneity of tumor-targeted protein nanoparticles. Nanoscale 2017;9:6427-35.

[46] Vincenzi B, Armento G, Spalato Ceruso M, Catania G, Leakos M, Santini D, et al. Drug-induced hepatotoxicity in cancer patients - implication for treatment. Expert opinion on drug safety 2016;15:1219-38.

[47] Sarges P, Steinberg JM, Lewis JH. Drug-Induced Liver Injury: Highlights from a Review of the 2015 Literature. Drug safety 2016;39:801-21.

[48] Damodar G, Smitha T, Gopinath S, Vijayakumar S, Rao Y. An evaluation of hepatotoxicity in breast cancer patients receiving injection Doxorubicin. Annals of medical and health sciences research 2014;4:74-9.

[49] Wang J, Wu Y, Dong M, He X, Wang Z, Li J, et al. Observation of hepatotoxicity during long-term gefitinib administration in patients with non-small-cell lung cancer. Anticancer Drugs 2016;27:245-50.

[50] Wang W, Lie P, Guo M, He J. Risk of hepatotoxicity in cancer patients Treated with immune checkpoint inhibitors: a systematic review and meta-analysis of published data. Int J Cancer 2017.

[51] Elefsiniotis IS, Pantazis KD, Ilias A, Pallis L, Mariolis A, Glynou I, et al. Tamoxifen induced hepatotoxicity in breast cancer patients with pre-existing liver steatosis: the role of glucose intolerance. European journal of gastroenterology & hepatology 2004;16:593-8.

[52] Bertrand N, Leroux JC. The journey of a drug-carrier in the body: an anatomo-physiological perspective. Journal of controlled release : official journal of the Controlled Release Society 2012;161:152-63.

[53] Regard JB, Sato IT, Coughlin SR. Anatomical profiling of G protein-coupled receptor expression. Cell 2008;135:561-71.

[54] Weiss ID, Jacobson O. Molecular imaging of chemokine receptor CXCR4. Theranostics 2013;3:76-84.

[55] Deslandes A. Comparative clinical pharmacokinetics of antibody-drug conjugates in first-in-human Phase 1 studies. mAbs 2014;6:859-70.

[56] Serna N, Sanchez-Garcia L, Sanchez-Chardi A, Unzueta U, Roldan M, Mangues R, et al. Protein-only, antimicrobial peptide-containing recombinant nanoparticles with inherent built-in antibacterial activity. Acta biomaterialia 2017.

[57] Wang AZ, Langer R, Farokhzad OC. Nanoparticle delivery of cancer drugs. Annual review of medicine 2012;63:185-98.

[58] Rueda F, Cespedes MV, Sanchez-Chardi A, Seras-Franzoso J, Pesarrodona M, Ferrer-Miralles N, et al. Structural and functional features of self-assembling protein nanoparticles produced in endotoxin-free Escherichia coli. Microbial cell factories 2016;15:59.

[59] Cano-Garrido O, Cespedes MV, Unzueta U, Saccardo P, Roldan M, Sanchez-Chardi A, et al. CXCR4(+)-targeted protein nanoparticles produced in the food-grade bacterium Lactococcus lactis. Nanomedicine 2016;11:2387-98.

Acknowledgments. We are indebted to Agencia Estatal de Investigación (AEI) and to Fondo Europeo de Desarrollo Regional (FEDER) (grant BIO2016-76063-R, AEI/FEDER, UE), AGAUR (2014SGR-132) and CIBER-BBN (project NANOPROTHER) granted to AV, Marató de TV3 foundation (TV32013-3930) and ISCIII (PI15/00272 co-founding FEDER) to EV and ISCIII (PI15/00378 and PIE15/00028, co-founding FEDER), Marató de TV3 foundation (TV32013-2030) and AGAUR 2014-PROD0005 to RM. Protein production has been partially performed by the ICTS "NANBIOSIS", more specifically by the Protein Production Platform of CIBER-BBN/ IBB (http://www.nanbiosis.es/unit/u1-protein-production-platform-ppp/). Biodistribution studies were performed in the NANBIOSIS Nanotoxicology Unit and particle characterization was partially done at the NANBIOSIS Biomaterial Processing and Nanostructuring Unit. We are also indebted to SCAC (UAB) for cell culture facilities and assistance. LSG was supported by AGAUR (2017FI_B100063), NS by a predoctoral fellowship from the Government of Navarra, UU received a Sara Borrell postdoctoral fellowship and MVC is supported by Miguel Servet contract, both from ISCIII and AV an ICREA ACADEMIA award.

Competing interests. LGS, NS, UU, MSC, IC, RM, EV and AV are con-inventors of the patent application EP17169722.0 on the use of self-structured protein drugs.